Radiography Studies for Proton CT

M. Petterson, N. Blumenkrantz, J. Feldt, J. Heimann, D. Lucia, H. F.-W. Sadrozinski, A. Seiden, D. C. Williams
SCIPP, UC Santa Cruz, CA 95064 USA
V. Bashkirov, R. Schulte
Loma Linda University Medical Center, CA 92354 USA
M. Bruzzi, D. Menichelli, M. Scaringella, C. Talamonti
INFN and Univ. of Florence, Italy
G.A. P. Cirrone, G. Cuttone, D. Lo Presti, N. Randazzo, V. Sipala
INFN Sezione di Catania, , I-95123 Catania, Italy

Abstract
We report the results of two beam experiments to develop proton Computed Tomography (pCT). The set-up consists of telescopes of silicon strip detectors at the entrance and exit of a segmented phantom to predict the path of the proton within the phantom and of a crystal calorimeter to measure the proton energy loss with high precision. The energy loss permits calculating the integrated proton stopping power along each proton path from which the electron density distribution can be reconstructed. We describe the 2D-image reconstruction of a low-contrast extended phantom, derive the relationship between contrast, feature size and dose, and study the spatial resolution achievable with this set-up.

I. Introduction

Proton radiation therapy is one of the most precise forms of non-invasive image-guided cancer therapy. It is based on the well defined range of protons in material, with low entrance dose, a dose maximum ("Bragg peak") and a rapid distal dose fall-off, providing better sparing of healthy tissue and allowing higher tumor doses than conventional radiation therapy with photons. At present, the potentials of proton therapy cannot be fully exploited because the conversion of Hounsfield values, measured with x-ray computed tomography (CT), to relative electron density values is not always accurate [1]. The resulting uncertainties can lead to range errors from several millimeters up to more than 1 cm depending on the anatomical region treated. Additional uncertainties exist with respect to the target position relative to normal tissues in the treatment room that could be minimized by using proton CT for guiding the therapy.

The long-term goal of our project is to develop the capability to use proton CT (pCT) instead of x-ray CT to minimize these uncertainties from the current value of 3-10mm to 1-3 mm. Previous work reviewed in [2] and our own preliminary studies [3-9] indicate that proton CT based on tracking of individual protons traversing an object from many different directions and measuring their energy loss and scattering angle may yield accurate reconstructions of electron density maps with good density and spatial resolution, despite the fundamental limitation of Multiple Coulomb Scattering (MCS).

II. PCT: Measurement Principle and Limitations

The requirement to measure single protons leads to the following conceptual design of the pCT scanner, shown in Fig. 1.a: the proton locations and directions at the entrance and exit of the phantom/patient are measured each with a telescope consisting of two x-y planes of silicon detectors. The energy is measured in a hodoscopic array of calorimeter crystals. Details are given in Ref. [8].

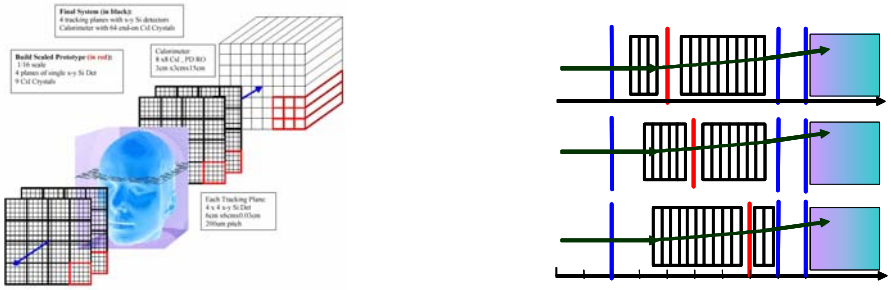

Fig. 1. a) Principle of the PCT system. b) Sketch of the beam set-up: the 200MeV proton beam enters from left, is maesured in the entrance silicon planes, passes through the segmented absorber (12 pieces of PMMA of 1.25 cm thickness each), and is again tracked in the exit telescope before being stopped in the crystal. For the tracking studies, the roving silicon module is located at 3 positions within the absorber stack. For the calorimeter studies, the front is also equipped with a telescope, and the phantom and a roving module are placed in the middle of the PMMA stack.

The challenge of proton-by-proton pCT can be evaluated by a comparison with its established alternative, x-ray CT. A detection of individual protons requires a data acquisition system capable of recording particle rates in excess of 1 MHz. We

have developed such a system for the readout of silicon strip detectors [9]. The curved trajectories of the protons inside the phantom create difficulties for the image reconstruction as well, and instead of a straightforward Filtered Back Projection (FBP) algorithm, a layer-by-layer de-convolution has been employed [10], [11].

Protons are undergoing Multiple Coulomb Scattering (MCS), which changes the direction depending on the amount of material traversed and the proton energy. The theory of MCS is well understood [12] and using it, the most likely path (MLP) inside the absorber can be reconstructed when the entrance and exit trajectories are measured external to the absorber. An analytical calculation of the MLP as a function of material, depth, displacement and scattering angle has been derived in [6] but needed to be verified experimentally. The results of this experiment [13] are reviewed briefly in the first part of this paper.

While x-ray CT uses a statistical evaluation of the absorption, pCT measures the energy loss of individual protons. In previous studies we showed high contrast imaging using 140 MeV protons [3]. The dose is proportional to the square of energy resolution (see below), thus mandating good energy determination. A recent beam test to measure the achievable contrast resolution and the implications for the dose and resolved feature size is described in the second part.

III. Beam Experiment Results: Tracking the Most Likely Path

The theoretical MLP prediction (MLP) and associated one sigma and 2-sigma envelopes [6] use the well established Gaussian approximation of multiple scattering theory [12]. The MLP depends both on displacement and exit angle. For typical MLPs the expected uncertainty is of the order of 300 μm. The objective of the tracking studies presented here was to verify the theoretical predictions by tracking individual protons inside a segmented absorber.

A beam experiment with 200MeV protons was performed at the Loma Linda University Medical Center (LLUMC) synchrotron. The protons were tracked with silicon strip detectors (SSDs) used before in the 1997 GLAST beam test [14]. In addition, a CsI calorimeter crystal provided energy measurement and a trigger for readout of the Si detector system.

A. Experimental Set-Up

Details of the experimental set-up and the data analysis are given in Refs [15], [16] and [17]. The set-up consisted of x-y silicon modules used as entrance and exit telescopes, and a CsI calorimeter (Fig. 1b). The set-up was flexible in that it allowed for insertion of up to 12 absorber plates (1.25 cm PMMA each) and a roving module between the telescopes. Data were taken both without absorber (to check the dispersion), and with absorber to map out the MLP at different depths within the PMMA stack with the roving module. The three different locations of the roving module at 3.75 cm, 6.25 cm and 12.5 cm depth of PMMA, are shown in Fig. 1. The beam diagnostic configuration allowed measuring the entrance location and angle of the protons, i.e. the beam size and beam spread, while the MLP determination set-up measured only the entrance location and not the entrance angle of the proton. Since the MCS angle turned out to be much larger than the beam spread, this was an acceptable solution.

B. Most Likely Path as a function of exit displacement and exit angle

The MLP analysis correlates the displacement in the roving module (i.e. position relative to the entrance position) with the exit displacement and angle. The displacements in the roving module are determined for bins of ± 200 μm in displacement at the material exit and ± 5 mrad in exit angle, respectively. Exit angles ranged from -80 mrad to +80 mrad. For comparison between the measured displacements and the theory the original MLP predictions for uniform medium was modified to include the air gaps of about 1.5 cm in our set-up allowing for insertion of the silicon detectors. Fig. 2.a shows the displacements in the roving modules located at different depths within the absorber for a few selected exit displacements and the prediction of the MLP calculated for the means in displacement and angle.

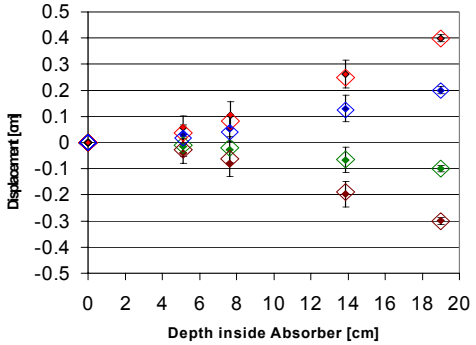

z [cm]	Exp No angle correction	Exp with angle correction	Theor. MLP
5	370	340	250
7.5	480	410	330
14	450	400	280

Fig. 2 Results from the tracking study: a) Comparison of the displacement measured in the roving plane at different absorber depths for 4 different exit displacements (shown at 18 cm depth) with the analytical calculation of the most likely path MLP (open symbols: the size of the symbol is close to the MLP spread). B) comparison of the RMS between the experiment with and without using the exit angle and the prediction of the MLP, all for an exit displacement of -0.4 cm.

The experimental data for an exit displacement of -0.4 cm are shown with their RMS variations, and the approximate spread in the theoretical prediction is indicated by the size of the symbols used. The prediction of the MLP is verified by the data within less than 200 μm, much less than the experimental spreads.

C. Spread in the Displacement Distributions within the Absorber

There are three different effects that can influence the spread in the roving modules. As mentioned before, the finite beam spread influences the spread of the experimental distributions. This has to be simulated with a full Monte Carlo program. Another is the bin size of the exit displacement selected. The third is introduced when defining the exit angle.

Both the experimental spreads and the expected MLP spread are constant at a constant roving location for all displacements at the absorber exit. The spreads in the roving modules are shown in Fig. 2.b. A marked reduction of the spread of the displacement in the roving module was observed when the information provided by the exit angle was used.

Since the exit angle spans range of about 50 mrad for every displacement the use of the exit angle in determining the roving position can result in a correction of about 300 to 500 μm, depending on the PMMA depth. Dividing the data into bins in angle reduces the experimental RMS of the roving displacements as shown in Fig. 2.b.

D. Agreement between data and the MLP calculation

The agreement between the data and the MLP calculation (modified for the finite air gaps at the position of the roving modules) has been tested for several exit displacements and angles. It was confined to values in these two parameters which contain about 80% of the data. The data were binned into bins of ± 200 μm in displacement at the material exit and ± 5 mrad in exit angle. There is agreement between the experimental displacement and the MLP prediction within about 350 μm, with growing disagreement at larger exit angles. We have started a Monte Carlo (MC) study of the experiment and a comparison between the MLP calculation and the complete MC results including the beam characteristics and the resolution of the detectors The study [18] indicates good agreement at small angles, and is now extended to large angles.

The beam test proves that already at this stage, the location of the proton within the phantom/patient can be predicted to better than 0.5 mm, validating the MLP approach which uses only **external** track information for the prediction of the trajectories **inside** the phantom/patient.

IV. CALORIMETER TEST

Since the integrated stopping power is determined from the energy loss, understanding the calorimeter response is of outmost importance for the pCT system. A dedicated test beam run was performed at LLUMC with essentially the same set-up as shown in Fig. 1.b, but with a "phantom" absorber as 6th plate and a roving module behind it. The phantom had holes drilled into it as shown in Fig. 4.a. Details of the analysis are given in [19].

A. Calorimeter response

The calorimeter response was determined with no PMMA absorbers at beam energies of 200 and 100 MeV, and pedestal runs without beam. The corresponding energy spectra are shown in Fig. 3.

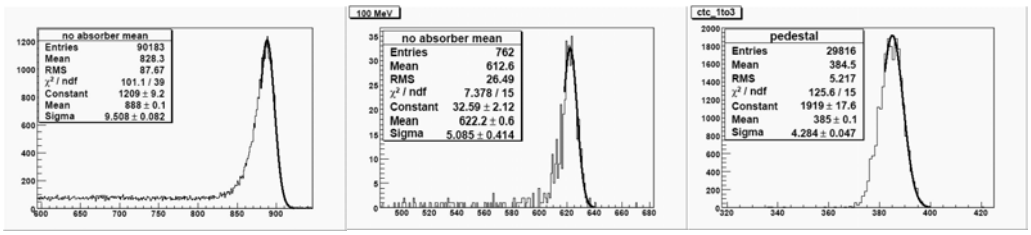

Fig. 3. Energy spectra (in CTC #) in the CsI calorimeter for beam energy a) 200 MeV, b) 100 MeV, and c) 0 (pedestal). The results of the Gaussian fits shown as solid lines are in the inserts.

Because of the tails in the distribution, only the high-energy part of the peak was fit to a Gaussian, yielding the mean E_m. The resulting calibration between the CTC value and the energy E of the proton (in MeV) at the calorimeter is almost linear and of the form $CTC\# = .0002 * E^2 + 2.5273 * E + 384.5$. The RMS of the Gaussian is the energy resolution σ_E, shown in Fig. 4. The energy resolution of the protons after traversing 12 or 11 planes of PMMA is about σ_E = 4 MeV, indicating that the energy straggling in the PMMA is the largest effect in the energy resolution for a crystal calorimeter.

B. Image Reconstruction

The images are reconstructed by defining pixels within a 2D grid in the silicon strip detectors, construct an energy spectrum

similar to Fig. 3 for each pixel in the grid, and plotting the fitted mean energy E_m in the pixel coordinates. In the following we selected as pixel size 5 strips x 5 strips (about 1.2 mm x 1.2 mm), and in addition voxels of 5 mm x 5 mm and 8 mm x 8 mm, respectively to approximately match the area and depth of the two types of large holes in the phantom. The result for the 5 strip x 5 strip pixels are shown in Figs. 4.b and 4.c. The images of the ½" and the ¼" hole in the phantom can be clearly seen on the background. For the analysis of the required dose for contrast and feature size, the areas inside the black boxes were chosen as the target and control voxels, respectively. The requirement of fitting the energy spectra has two consequences: if the number of protons in one pixel is lower than 10, a reliable fit could not be performed. These pixels are shown in white in the 2D images. In addition, only about ¼ of all events in a spectrum contribute to the determination of the mean energy.

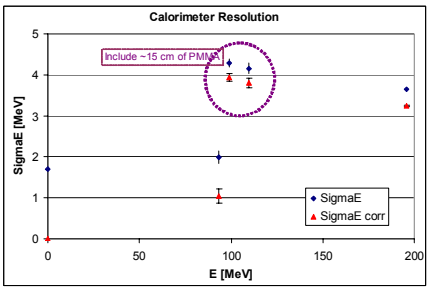

Fig. 4. Energy resolution σ_E in the CsI calorimeter as a function of energy. Both the RMS as measured and corrected for the pedestal are shown.

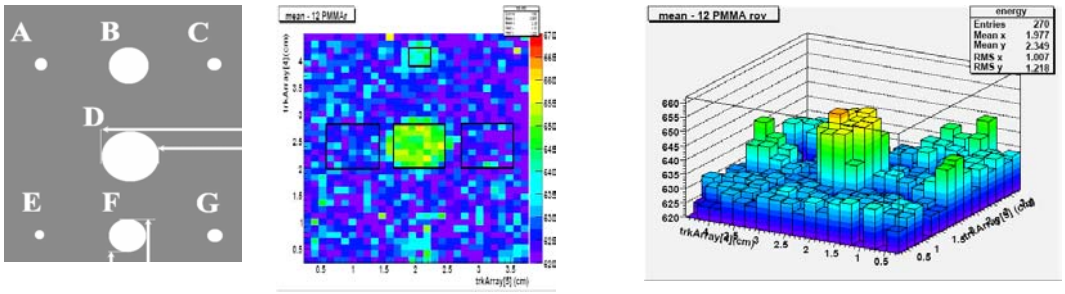

Fig. 5. Image of the phantom: a) location of the holes, b) 2D figure of the reconstructed energy with black boxes indicating the location of the target voxels and the control regions (pixel size 1.2 mm x 1.2 mm). c) 3D figure of the reconstructed energy with 2.4 mm x 2.4 mm pixels.

C. Required Dose as a function of contrast and feature size

Proton imaging is based on differences in local energy loss in the phantom. Locally, the stopping power is proportional to the density ρ inside the voxels, and thus the contrast between two voxels is given by the product of density difference Δρ and the voxel size d. The energy measurement is used to resolve this contrast. The significance S of the energy measurement between two voxels is the ratio of the difference of the energy means $\Delta E_m \propto \Delta\rho \cdot d$ and the error on the measurement σ_m.

$$S = \Delta E_m / \sigma_m$$

For a Gaussian or Poisson distribution, $\sigma_m = \sigma_E / \sqrt{N}$. We will ask for a minimum of 2 sigma significance, S=2 :

$$\Delta E_m = 2\sigma_m = 2\sigma_E / \sqrt{N}$$

The dose D is given by the deposited energy, and thus related to the proton fluence Φ = $N_p / Area$ and the local stopping power dE/dx.

$$D \propto N_p / d^2$$

where d is the size of the pixel. As mentioned above, the number N of protons contributing to the Gaussian fit is about ¼ of the total number of protons N_p contributing to the dose. The dose dependence on feature size d, energy resolution σ_E and contrast (density variation) Δρ is

$$D \propto \frac{\sigma_E^{\,2}}{\Delta^2 \rho \cdot d^3}$$

We have used the beam test data to investigate the validity of some of the assumptions made above. In Fig. 7, the assumptions $\sigma_m = \sigma_E / \sqrt{N}$ has been tested as a function of the fluence reduction factor n. We find fairly good agreement within 50%. In Fig. 8, the need for a significance of at least 2 is shown, since for less significance the image of the large voxel can't be distinguished anymore.

In fig. 9 the required dose for two different voxel sizes and density variation of Δρ = 1.2 g/cm^3 is shown. The two measurement scale with the expected d^{-3} dependence. In addition the lower dose limit from the requirement to have at least 10 protons for the fit of the energy spectrum is shown. These values will be used as input for the dose calculations in image

reconstruction studies.

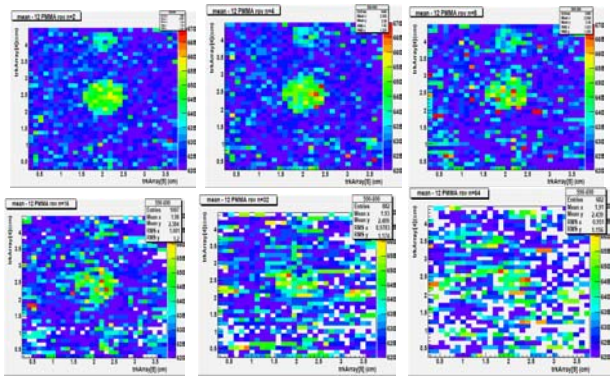

n	1	2	4	8	16	32	64	128
# entries voxel	5598	2758	1374	671	337	174	92	52
#entries per 5sx5s pixel	114.24	56.3	28.04	13.694	6.878	3.55	1.8776	1.0612
# entries control L	6377	3196	1609	797	394	207	87	38
#entries per 5sx5s pixel	130.14	65.2	32.84	16.265	8.041	4.22	1.7755	0.7755
# entries control R	2629	1297	640	321	148	78	40	26
#entries per 5sx5s pixel	53.653	26.5	13.06	6.551	3.02	1.59	0.8163	0.5306

Fig. 6. a) Image of the phantom in 1.2 mm x 1.2 mm pixels: a) with progressively larger fluence reduction factor n, from n=2 to 64. b) Number of protons in the selected areas and inside the 1.2 mm x 1.2 mm pixels. The image for n=16 is much blurred and shows many white pixels where no valid fit could be performed, and thus indicates the non acceptable limit.

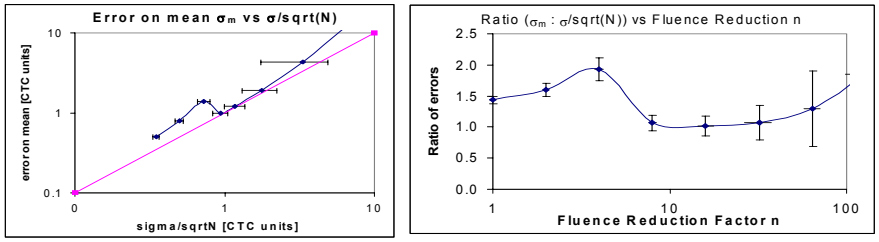

Fig. 7.a) Correlation between the expected energy error $\sigma_E / \sqrt{N}$ and the error on the mean energy from the Gaussian fit σ_m. b) Ratio between error on the mean energy σ_m and the expected value $\sigma_E / \sqrt{N}$ as a function of the fluence reduction factor n. Ideally, this ratio should be unity.

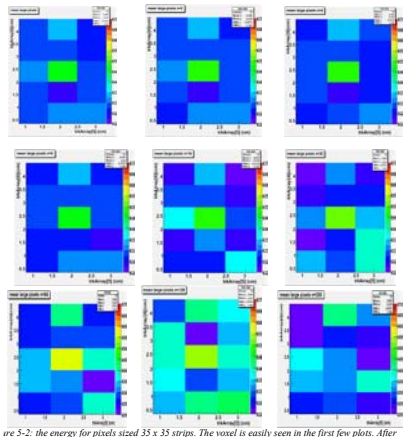

n	# entries voxel	mean	error on mean	# entries control	mean control	Significance
1	5598	655	0.5	6377	629.4	51.2
2	2758	654	0.8	3196	629.3	30.875
4	1374	652.2	1.4	1609	629.3	16.357143
8	671	652.40	1.00	797	628.5	23.9
16	337	652.60	1.20	394	628.7	19.916667
32	174	655.50	1.90	207	628.4	14.263158
64	92	655.60	4.30	87	632	5.4883721
128	52	654.40	11.70	38	634.2	1.7264957
200	19	630.70	12.30	24	635	-0.35

ure 5-2: the energy for pixels sized 35 x 35 strips. The voxel is easily seen in the first few plots. After

Fig. 8. Image of the phantom in 8 mm x 8 mm pixels: a) image with progressively larger fluence reduction factor from n =1 to 200, b) effect of fluence reduction on the energy mean and the significance of the energy measurement. The limit is reached at about n=100, where the target voxel becomes indistinguishable from the background.

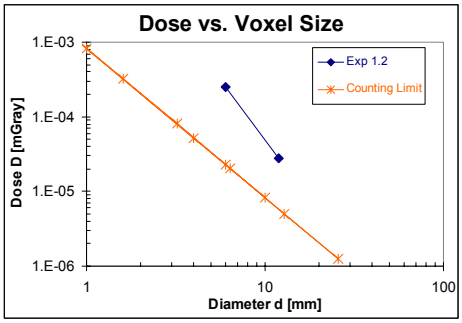

Fig. 9. Dose – feature size relationship for the experimental contrast $\Delta\rho = 1.2$ g/cm^3. The dose ratio for the two measured voxel is 0.11, while the expected ratio from the d^{-3} dependence is 1.1. The line labeled "counting limit" is based on the fact that the energy determination requires at least 10 protons.

V. Conclusions

We have measured the most likely path of 200 MeV protons inside a segmented absorber of PMMA. The displacements of the protons from their original path agree well with the theory of multiple Coulomb scattering (MCS). We show that as expected from the theory of the most likely path (MLP) [6], we can predict the trajectory of the proton inside the absorber to better than 0.5 mm.

We have imaged a low-contrast phantom inside a stack of PMMA plates and reconstruct the mean energy through fits of the energy spectra within a pixel. The images require at least 2 sigma significance of the energy measurement. By reducing the fluence within the data we extract a minimum dose level for a density variation of 1.2 g/cm^3 and voxel size of 1.2 and 6 mm, which agrees well with th expected d^{-3} behavior. In addition, a minimum dose level for any contrast is derived based on the minimum number of protons required fit the energy spectrum.

VI. Acknowledgment

We appreciate the smooth running of the LLUMC synchrotron.

References

[1] B. Schaffner and E. Pedroni, "The precision of proton range calculations in proton radiotherapy treatment planning: experimental verification of the relation between CT-HU and proton stopping power", *Phys Med Biol*. 43(6):1579-1592, 1998.

[2] H. F.-W. Sadrozinski, V. Bashkirov, B. Keeney, L. R. Johnson, S. G. Peggs, G. Ross, T. Satogata, R. W. M. Schulte, A. Seiden, K. Shanazi, and D. C. Williams, "Toward proton computed tomography", *IEEE Trans. Nucl. Sci*, vol 51, no.1, pp. 3-10, Feb. 2004.

[3] L. R. Johnson, B. Keeney, G. Ross, H. F.-W. Sadrozinski, V. Bashkirov, R. W. Schulte, K. Shahnazi. "Initial studies on proton computed tomography using a silicon strip detector telescope", *Nucl Instr Meth* **A** 514 (2003) 215.

[4] HF-W Sadrozinski, M. Bruzzi, L.R. Johnson, B. Keeney, G. Ross, A. Seiden, D. C. Williams, L. Zhang, V. Bashkirov, R. W. Schulte, K. Shahnazi. "Issues in proton computed tomography", *Nucl Instr Meth* **A** 511: (2003) 275-281.

[5] L. R. Johnson, B. Keeney, G. Ross, H. F.-W. Sadrozinski, A. Seiden, D. C. Williams, L. Zhang,V. Bashkirov, R. W. Schulte, K. Shahnazi, "Monte Carlo studies on proton computed tomography using a silicon strip detector telescope". SCIPP 02/35.

[6] D C Williams, "The most likely path of an energetic charged particle through a uniform medium", *Phys. Med. Biol*. 49 2899-2911, 2004.

[7] R. W. Schulte, V. Bashkirov, M. C. Klock, T. Li, A. J. Wroe, I. Evseev, D. C. Williams, T. Satogata, "Density resolution of proton computed tomography", *Med Phys. 2005, 32:1035-46.*

[8] R. W. Schulte, V. Bashkirov, T. Li, Z. Liang, K. Mueller, J. Heimann, L. R. Johnson, B. Keeney, H. F.-W. Sadrozinski, A. Seiden, D. C. Williams, L. Zhang, Z. Li, S. Peggs, T. Saratoga, C, Woody, "Conceptual design of a proton computed tomography system for applications in proton radiation therapy", *IEEE Trans. Nucl. Sci., vol 51, no.3, pp 866 – 875, June 2004.*

[9] H. F.-W. Sadrozinski, V. Bashkirov, M. Bruzzi, M. Ebrahimi, J. Feldt, J. Heimann, B. Keeney, F. Martinez-McKinney, D. Menichelli, G.Nelson, G. Nesom, R. W. M. Schulte, A. Seiden, E. Spencer, J. Wray, and L. Zhang, "The particle tracking silicon microscope PTSM", *IEEE Trans. Nucl. Sci., vol* 51, no.5, pp 2032 – 2037, Oct 2004.

[10] T. Li, Z. Liang, et al. " Reconstruction with most likely trajectory for proton computed tomography", *SPIE Medical Imaging*, 2004.

[11] T Li, Z. Liang, K. Mueller, J. Heimann, L. Johnson, H. F.-W. Sadrozinski, A. Seiden, D. Williams, L. Zhang, S. Peggs, T. Satogata, V. Bashkirov, and R. W. Schulte, "Reconstruction for proton computed tomography: a Monte Carlo study", *IEEE NSS/MIC Conf Record* 2003.

[12] Particle Data Group, S. Eidelman et al., "Review of Particle Physics", *Physics Letters* B 592, 1 (2004).

[13] Nate Blumenkrantz, Jason Feldt, Jason Heimann, Hartmut F.-W. Sadrozinski, H. F.-W. Sadrozinski, , A. Seiden, et al."Prototype Tracking Studies for Proton CT ", accepted for publication in, *IEEE Trans. Nucl. Sci.*.

[14] W. B. Atwood, S. Ritz, P.Anthony, R.P.Johnson, W.Kroeger, H.F.-W.Sadrozinski et *al.,* "Beam test of Gamma-ray Large Area Space Telescope components", *Nucl.Instrum.Meth*. A446 (2000) 444-460.

[15] J. Heimann, "Developing an FPGA-based Readout for the pCT Detector System", Senior Thesis, UC Santa Cruz Physics Dept., June 2005.

[16] J. Feldt, "Preliminary Tracking Studies for Proton CT", Masters Thesis, UC Santa Cruz Physics Dept., December 2005.

[17] N. Blumenkrantz, "Tracking Study of 200 MeV Protons within a PMMA Phantom", Senior Thesis, UC Santa Cruz Physics Dept., March 2006

[18] G. A. P. Cirrone et *al*, "Detailed Monte Carlo Investigation of a Proton Computed Tomography System", Poster J03-25, 2005 IEEE NSS-MIC Symposium in Puerto Rico, Oct 2005.

[19] M. K. Petterson, "Calorimeter Studies for Proton pCT", Senior Thesis, UC Santa Cruz Physics Dept., June 2006.